Nanoscale

Accepted Manuscript

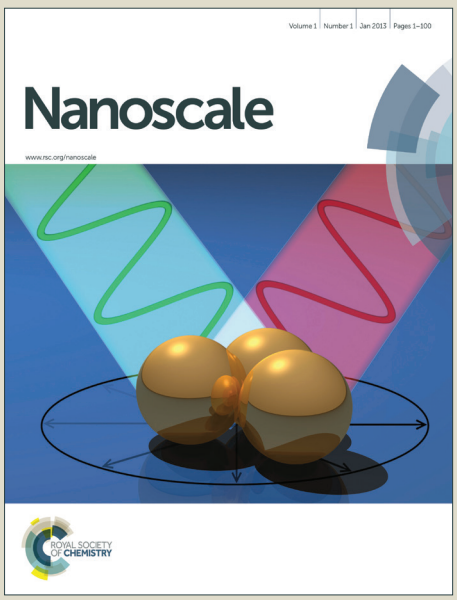

ROYAL SOCIETY OF CHEMISTRY

www.rsc.org/nanoscale

Anti-epidermal growth factor receptor conjugated mesoporous zinc oxide nanofibers for breast cancer diagnostics†

Md. Azahar Ali[$a], Kunal Mondal[$a], Chandan Singh[b], Bansi D. Malhotra[#c] and Ashutosh Sharma*[a]

[a]Department of Chemical Engineering, Indian Institute of Technology, Kanpur, India
[b]Department of Science and Technology Centre on Biomolecular Electronics, Biomedical Instrumentation Section, CSIR-National Physical Laboratory, New Delhi, India
[c]Department of Biotechnology, Delhi Technological University, Delhi, India

We report fabrication of an efficient, label-free, selective and highly reproducible immunosensor with unprecedented sensitivity (femto-molar) to detect the breast cancer biomarker for the early diagnostics. Mesoporous zinc oxide nanofibers (ZnOnF) are synthesized by electrospinning technique with fiber diameter in the range of 50–150 nm. Fragments of ZnOnF are electrophoretically deposited on indium tin oxide substrateand conjugated via covalent or electrostatic interactionswith a biomarker (anti-ErbB2; epidermal growth factor receptor 2). Oxygen plasma treatment of carbon doped ZnOnF generates functional groups (-COOH, -OH *etc.*) that are effective for the conjugation of anti-ErbB2. ZnOnF without plasma treatment that conjugate via electrostatic interaction were also tested for comparison. Label-free detection of breast cancer biomarker by this point-of-care device is achieved by electrochemical impedance technique with a high sensitivity (7.76 kΩ/μM) and can detect 1fM (4.34×10^{-5}ng/mL) concentration. Excellent impedimetric response of this immunosensor provides a fast detection (128 s) in a wide detection test range (1.0 fM-0.5 μM). Oxy-plasma treated ZnOnF immunoelectrode shows higher association constant (404.8 $kM^{-1}s^{-1}$) indicating higher affinity towards ErbB2 antigen compared to the untreated ZnOnF immunoelectrode (165.6 $kM^{-1}s^{-1}$). This sensor is about an order more sensitive than the best demonstrated in the literature based on different nanomaterials and about three orders of magnitude better than ELISA standard for breast cancer biomarker detection. The proposed point-of-care cancer diagnostics offers several advantages such as higher stability, rapid monitoring, simplicity, cost-effectiveness, *etc.* and should prove to be useful for the detection other bio- and cancer markers.

KEYWORDS: Point-of-care device, Oxy-plasma treatment, Breast cancer biomarkers, Mesopore, Zinc oxide nanofibers, Electrospinning, Label-free detection.

***Corresponding Authors:** bansi.malhotra@gmail.com[#] and ashutos@iitk.ac.in[*]; [$]These authors have contributed equally.

†Electronic supplementary information (ESI) available.

Introduction

With recent advances in genomics, proteomics and molecular pathology, the detection of cancer biomarkers for the investigation of the genetic changes during malignant transformationsis found to be an interesting tool.[1] Cancer biomarkers are the chemical substancesthat are related to malignant tumors and can be found in blood, urine, stool, other bodily fluids, or tissues of affected patients.[2,3] The growth factor receptors, peptide growth factors, signal transduction factors, tyrosine kinase, and transcription- regulatory proteins are over-expressed in cancer cells. In particular, the human epidermal growth factor receptor (EGFR or ErbB2) has been found in around 33% of breast cancers.[4, 5] The ErbB2 gene is found on 17q chromosome and encodes for 185-kDa transmembrane tyrosine kinase growth factor receptor.[6] The discovery of ErbB2 gene amplification, its overexpression in primary breast cancer and most importantly, its association with more aggressive clinical behavior makes ErbB2 a highly suitable candidate for diagnostics application.

The most widespread tools of breast cancer detection are X-ray mammography and ultrasound to investigate the density changes in the breast.[7] Although magnetic resonance imaging technique is a highly sensitive tool, it lacks specificity. Besides this, early diagnostics and cost are major concerns for the quantification of cancerous molecules. Thus,the biosensor devices[8]are considered to play an important role in the early detection of breast cancer molecules, since it offers low cost, fast detection, portability, absence of side-effects, *etc.*It is known that the antigen and antibody of epidermal growth factor receptor in a cancer cell provides specific biding sites (paratope and epitope) that allows development of biosensor devices to detect cancerous molecules.[9] For example, antibody conjugated quantum dots have

been utilized for the detection of HER2 biomarker in lung and breast cancer cells[8]and Yong *et al.* fabricated bioconjugated indium phosphide (core)-zinc sulfide (shell) quantum dot nanoprobes for quantification of cancer molecules via imaging technique.[10] Akter *et al.* have developed an electrochemical immunosensor based on multi walled carbon nanotubes and gold nanocomposites for the amplified detection of prostate specific antigen.[9]

The application of nanostructured materials has grown rapidly in biomedical fields including molecular imaging, *in vitro* cancer cell studies, early diagnostics, and personalized treatment of cancer.[11] One dimensional (1D) nanorods, nanowires, and nanofibers of zinc oxide (ZnO) have been predicted to have considerable potential for biomedical applications including DNA delivery, bioimaging, magnetic resonance imaging, nanoelectronics and biosensors devices due to its higher surface-to-volume ratio, excellent electron transfer communication, environmental safety, biocompatibility, nontoxicity, chemical stability, and biodegradability.[12-16] The anisotropic structure of ZnO is known to exhibit higher electron mobility and diffusion co-efficient compared to other metal oxides like titanium oxide.[17] Nanofibers of ZnO due to their high surface-to-volume and aspect ratios can play an important role for electrochemical biosensors.[13] Zinc oxide nanofibers (ZnOnF) may provide an electrical conduction path between proteins and electrode that enhance charge transfer properties resulting in higher sensitivity of the biodevices. Thus, there has been a rapid growth in the literature on the application of nanopore metal oxides including ZnO for the detection of various biomolecules such as glucose, DNA, antibodies and bacteria with improved stability and selectivity.[18] The nanopore structures result in improved analytical performance due to higher loading of active catalysts and higher diffusion rates.[19] The nanopore ZnO is found to be most stable because of its highly cross-linked structure that may resist biodegradation.[20] Thus, the pore size, shape,

hydrophilicity/hydrophobicity, charge distribution, pH environment and conductivity of ZnOnF for biosensor applications can be tuned by varying the composition of the material during its synthesis process.

The bioconjugation of protein molecules with a metal oxide surface has recently attracted much interest for the development of nanobioelectronic devices for point-of-care (POC) diagnostics.[21] Efforts have been made to identify the interaction of proteins molecules with the mesoporous metal oxides surface.[22] Some of the important factors associated with protein conjugation are the mesopore structured diameter, surface-to-volume ratio, morphology, surface modification, ionic strength, isoelectric point and protein dimension. Surface chemistry on a metal oxide can promote better conjugation of protein molecules by creation of functional groups.[23,24] Mesoporous 1D nanofibers are known to facilitate the attachment of protein biomarkers (antibodies) or DNA molecules due to their fascinating geometries that may provide numerous absorption sites onto the nanofibers surface.[25] For conjugation of biomolecules, the physical absorption driven by electrostatic attraction is a direct approach for attachment of biomolecules due to ZnOnF's higher isoelectric point (10.3) allowing it to easily bind with the low isoelectric point protein molecules (~1-5).[20] Although non-specific binding due to electrostatic interactions with foreign molecules may prove to be a disadvantage, this method has been widely explored. However, covalent interactions can overcome this limitation due to strong amide bondformation. Zinc oxide surface can be modified by surface treatment such as oxygen plasma, wet chemical, surface graft polymerization, co-electrospinning,*etc.*[14]Carbon doped in ZnO not only helps to create the surface functional groups but also improves the electrochemical performance of a biosensor.[12, 26] In addition, surface functional groups on ZnOnF surface in covalent interactions may amplify the electrochemical impedance signal. Xu*et al.* fabricated 1D

channel of ordered mesoporous metal oxide to assemble functional proteins for electrochemical detection of hydrogen peroxide.[27] Mondal *et al.* fabricated mesoporous metal-oxide nanofibers for the functionalization of cholesterol esterase and cholesterol oxidase enzyme molecules.[12] Hong *et al.* synthesized ZnO nanowires for fluorescent cancer cell imaging.[28] Ahmed *et al.*have fabricated a glucose biosensor using ZnOnF and obtained sensitivity (70.2 μA cm^{-2} mM^{-1}) for glucose detection.[13] Other nanostructured materials including carbon nanotubes,[29] reduced graphene oxide-SnO_2nanocomposite,[30] hydrazine coated gold nanoparticles[30] *etc*. have been used to detect cancer biomarkers. However, their limitation such as poor sensitivity and limit of detection can be improved by using porous morphology ZnOnF. The mesoporous1D ZnOnF has not been explored for the fabrication of POC devices for cancer biomarker detection till date.

Here we explore oxygen plasma treated and untreated electrospun mesoporous zinc oxide nanofibers (ZnOnF) platforms for conjugation with antibody of human epidermal growth factor receptor 2 (anti-ErbB2) and its use for the label-free detection of ErbB2 via antigen-antibody interactions. Precursor materials such as a carrier polymer (polyacrylonitrile; PAN) and zinc acetate are utilized for the synthesis of ZnOnF mats via electrospinning followed by calcination. Shape, size and diameter of nanofibers have been controlled by varying concentration of the precursor materials, solution viscosity, flow rate, applied electric field, *etc.* A small amount of residual carbon in the ZnOnF was optimized for creating functional groups to get best sensor performance by varying the calcination temperature. ZnOnF deposited on indium tin oxide are conjugated with anti-ErbB2 via covalent as well as physical electrostatic interactions. Owing to the residual carbon in ZnOnF, the oxygen plasma treatment generated the functional groups such as –COOH which make a strong amide bond (C-N) with protein molecules. The functional property of ZnOnF and their shape, size, crystalline structure, *etc.* have been investigated using

structural and morphological studies. Label-free detection of ErbB2 has been carried out using protein conjugated ZnOnF immunoelectrode via electrochemical impedance spectroscopic technique.

Results and discussion

Optimized Synthesis and Morphological Studies of ZnOnF. The synthesis of electrospun ZnO nanofibers was accomplished using a chemical method at a temperature of about 60 °C, including mixing of a metal acetate dihydrate salt, zinc acetate dihydrate (ZnA) with polar basic aprotic solvent (DMF) followed by a high temperature (500 °C) thermal treatment. The use of DMF as a useful reaction media for the arrested basic hydrolysis of zinc salts has been reported earlier.[31] In this approach, DMF controls the hydrolysis of zinc acetate dihydrates salt.[32] The carrier polymer (PAN) dissolved in DMF acted as a template and controls the growth kinetics of the ZnO. This precursor undergoes hydrolysis in the presence of moisture and forms ZnO gel in the electrospun nanofibers. The as-spun nanofibers mats were left in air for stabilization to permit the complete hydrolysis of ZnA. The PAN was removed by calcination leaving behind a continuous mesoporous ZnO nanofibers mat with some residual carbon content.

The vital parameters for electrospinning of PAN/ZnA were optimized by Singh *et al.*[33] to obtain uniform polymeric fibers with diameter in the range of 180–350 nm. The role of sacrificial polymer PAN in the electrospun solution was to increase the viscosity and therefore to control the viscoelastic behavior of the blend. The diameter of the electrospun nanofibers could be varied, which is a determining factor in the conductivity of the fibers and thereby increase the biosensing efficiency. The lower fiber diameter leads to higher specific surface area therefore ensuring more number of reaction sites for enhancing electrocatalytic efficacy. In order to optimize the diameter of the fibers, we have fixed the applied voltage, distance between the

collector and the needle tip, ambient properties like temperature, humidity while we varied electrospinning process parameters like polymer wt. % and flow rate of the solution.

Electrospinning of ZnO occurs because of the high DC potential applied between the needle tip and the grounded rotating electrode. Because of the high voltage, the polymer drop at the needle tip starts to elongate and a thin polymer jet was ejected when the applied electric field strength beats the surface tension of the polymer solution. Stretching of this viscoelastic polymeric filament under the electric field coupled with the rapid solvent evaporation produces nanofibers deposited on the grounded rotating electrode. The rotating drum collector was used here to change the alignment of the collected fibers. At low rpm (<500 rpm), the fibers were randomly deposited onto the collector surface. As the rotational speed of the drum was increased (usually >1000 rpm), fibers were collected on the drum surface in a partially aligned orientation.

The diameter and morphology of the as-spun and ZnOnF were confirmed by the field emission-scanning electron microscopy (FE-SEM) studies. It was observed that at the solution flow rate of 75 μL/min, the diameter of the PAN/ZnA fibers decreases with the reduction in the polymer concentration. The fibrous morphology is still retainedup to a lower critical polymer concentration ~ 2 wt.%. Below this concentration, electro-sprayed bead like structures were formed. A combination of beads and non-uniform fiber formation continues from 2 to 6 wt.% as revealed by FESEM micrograph (Figure1a). The formation of bead like structures occurs at low polymer wt.% which inhibits the Taylor cone formation. At low wt.% of PAN (low viscoelasticity of polymer solution), the liquid jet breakdowns easily and creates an electrospray of droplets/beads or beaded non-uniform PAN/ZnA fibers. Further increase in PAN concentration to7.5wt.% produces bead-free continuous fiber matofincreasing diameter (Figure1b,c). At very high polymer concentration of 14wt.%, thick roughnon-uniform diameter

fibers (average diameters ~ 0.85 μm) were obtained (Figure1d). Therefore, 7.5 wt.% PAN solution was found to be near optimal for producing bead-free, uniform diameter and nanofiber mats of fiber diameter around270 nm (calculated from Figure 1c).

When the flow rate of the PAN/ZnA solution (7.5 wt.%) was varied, the average fiber diameter was found as ~180 nm and ~650 nm for 15 μL/min and 150 μL/min, respectively (Figure 1e,f). In order to preserve the Taylor cone, the flow rate of solution needs to be optimized accordingly.[33] At very low flow rate (15 μL/min), dry polymerat the tip of the needle was produced (Figure 1e shows beaded non uniform fibers) whereas very high flow (150 μL/min) produced large droplets andthick beaded fibers (Figure 1f). Hence, it has been found that a 7.5 wt.% PAN/ZnA solution, a flow rate of 75 μL/min and 14 kV DC voltage applied between a rotating electrode and needle tip placed at 4 cm apart, produced near optimal thick nanofiber mats.

Structural and Electron Microscopic Studies. Figure 2 shows the morphology of the nanofibers after their calcination at 500 ^{o}C. Figure 2a shows the low magnification SEM image of a free-standing ZnOnF mat (calcined at 500 ^{o}C) consisting of partially aligned nanofibers. The as-spun nanofibers (Fig. 1b, c) are of smooth morphology, free from beads, uniform in diameter and are partially aligned in orientation. Calcination at 500 °C (Fig. 2b, c) produced mesoporous continuous long nanofibers with average diameter of about 80 nm. Approximately, 70% shrinkage in the fiber diameter was observed after calcination of 7.5wt.% PAN/ZnA blend electrospun at 75 μL/min flow rate. As calcination was optimized earlier[32], we calcined at 500 ^{o}C to retain a small amount of residual carbon within the ZnOnF mats which may play an important role for protein conjugation after the oxy-plasma treatment. Figure 2d and e describe the morphology of the ZnOnF after the loading of antibodies (anti-ErbB2). It is confirmed that

ZnOnF retain their fibrous morphology even after electrophoretic deposition (Figure 2d and e). After immobilization via surface treatment, the SEM image of the anti-ErbB2 covered ZnOnF surface is shown in Figure 2d. It can be seen that the plasma treated fibers show less propensity for aggregation. In addition, the mesopore structure of ZnOnF may enhance the absorption of protein molecules. The high resolution FESEM image after loading of the anti-ErbB2 molecules is shown in Figure 2e.

Elementary analysis for ZnOnF and fZnOnF films and with antibody functionalization has been carried out to confirm the presence of elements in the prepared samples. Figure S1(i, Supplementary Information)shows the energy dispersive X-ray (EDX) analysis spectra (embedded with the quantitative data) indicating removal of polymer with carbon present after calcination at 500°C for 4 h (a).After antibody functionalization, a peak EDX peak appears for carbon element (atomic ratio; 12.2%) indicating the presence of antibody molecules on ZnOnF surface. Figure S1 (ii, Supplementary Information) shows the EDX analysis spectra (embedded with the quantitative data) indicating removal of polymer with small amount of residual carbon present after calcination. After protein conjugation in the EDX spectra, the elements such as phosphorus (P), calcium (Ca), potassium (K) and chlorine (Cl) found in sample may be due to PBS with antibody on fZnOnF transducer surface [Figure S1(ii), Supplementary Information]. However, the atomic ratio of carbon elements is found to increase indicating biofunctionalization of antibody on fZnOnF transducer.

The microscopic structure of electrospun ZnOnF obtained after calcination was investigated by TEM studies. The diameter of calcined ZnOnF is around 60-120 nm after calcination at 500 ^{o}C. Figure 2f shows TEM images of ZnO fibers. It is easy to identify ZnO grains from the magnified image shown in the inset of Figure 2f. This suggests that the ZnOnF

crystallized sufficiently due to high temperature calcination. The average crystallite size of ZnO within the nanofibers is found to be ~32 nm by analyzing TEM micrographs (analyzed by image J software).Thediameter of the fiber shrinks down to about 80 nmby heat treatment. The grains of ZnO are produced from ZnA salt and grow by oxidation at high temperature calcination. The growth of the crystallites is along the fiber direction. It can be seen that the ZnO nanofibers contain small nanoparticles of ZnO along the fibers direction, however, inset shows nanostructured flower like ZnO wrapped along the (101) direction of ZnOnF confirmed by X-ray diffraction (XRD) studies.

The XRDstudies were conducted to investigate the crystalline structure of synthesized ZnOnF at a slow scan rate of 1°/min. Presence of various peaks in the XRD pattern [Figure 3i]indicate the wurtzite structure of crystalline zinc oxide with the peaks matched with JCPDS card no. 36-1451 (lattice parameters; a = 3.249 Å and c = 5.206 Å). The crystallite size of zinc oxide (calcinedat 500°C) was calculated as 35.35 nm for the (101) plane using the Debye–Scherrer equation. This indicates that the zinc oxide crystallites grow along (101) direction. A peak has been found for (002) reflection plane at 2θ=22.6˚ due to the residual of carbon content. In the UV-visible spectra, it can be seen that the absorption increases from 420 nm to 250 nm and maximum is at 350 nm due to the quantum confinement effect indicating the formation of nanostructured zinc oxide [Figure 3iii]. Estimated band gap (3.0 eV) of ZnOnF is reduced compared to bulk zinc oxide. Reduction of band gap for the synthesized zinc oxide nanofibers is due to the blue shift which may help inenhancing the electron conduction during electrochemical measurement.

To investigate the porosity of synthesized ZnOnF, we conducted the Brunauer–Emmett–Teller (BET) measurement. For sampling the specific surface area, the sample was degassed in

vacuum at 200°C for 8 h and then the nitrogen adsorption and desorption isotherms were recorded (Figure 3iv). The pore size distribution was analyzed using non-local density functional theory from the adsorption branch of the isotherm [Figure 3iv, inset]. The volume was calculated from the adsorbed nitrogen gas at relative pressure (P/P_o) of 0.9994. The total BET surface area was found ~28.07 m^2/g with the average pore diameterabout 14.41 nm and all the pores were below 326.9nm sizes. The pore volume was estimated by BJH desorption method as 10.11×10^{-2} cc/g where the micro, meso and macropore volumes were distributed around0.0115, 0.057 and 0.03 cm^3/g, respectively. Thus, the results indicate that ZnOnF consists of meso (57 %) and macropores (31.7 %) with a fraction of around 11 % microspores. The mesoporous structure of zinc oxide fibers may enhance the loading capacity of protein cancer biomarkers.

To confirm the available functional groups and formation of chemical bonding on ZnOnF surface, the FT-IR studies were performed (Figure 3ii). In the finger print region of the spectra, the peak seen at 533 cm^{-1} is due to Zn−O vibration bend in the sample. A wide absorption peak (curve a) was observed at 3357 cm^{-1}corresponding to Zn−OH stretching in ZnOnF sample. The strong absorption peak found at1100 cm^{-1} reveals presence of the O−C group in the surface of ZnOnF. The peak at 850 cm^{-1} indicates C−H bending in the finger print region of the sample. The characteristic peak at 1422 cm^{-1} is assigned to C−O−H bending while at 1500 cm^{-1} is assigned to the C=C bending. However, oxygen plasma treatment of ZnOnF surface changed the peak position toward higher wavenumber from 1100 cm^{-1} to 1130 cm^{-1}, and peak intensities were increased (curve b). A peak observed at 1649 cm^{-1} reveals the presence of the carboxyl group on fZnOnF due to oxygen plasma treatment indicating –COOH functionalized surface (Mondal *et al.*).[12] Additional peak found at 2070cm^{-1} is due to absorption of CO_2 on fZnOnF surface. After antibody (anti-ErbB2) functionalization on fZnOnF surface, the peaks as seen in spectra c and d

are found to disappear indicating the absorption of antibody on fZnOnF surface. A broad absorption peak found at 1040 cm^{-1} (curve d) due to C-N bending arises from the covalent interaction of –COOH groups and $–NH_2$ groups of fZnOnF and anti-ErbB2, respectively. In both spectra, at peak at 1631 cm^{-1}, which is due to N-H stretching of amide II bond, results after the antibody ErbB2 absorption on ZnOnF (c) and fZnOnF (d).

Electrochemical Properties. Cyclic voltammetric studies were conducted to investigate the electrochemical properties for mesoporous ZnOnF based electrodes in a wide potential range (-0.6 to 0.7 V). Curves show excellent oxidation and reduction peaks for the fabricated electrodes in the presence of $[Fe(CN)_6]^{3-/4-}$ mediator [Figure 4i]. The ZnOnF/ITO electrode shows an oxidation peak potential of 0.37 V and current at 426 μA. Surface oxy-plasma treatment on ZnOnF surface results in a decreased oxidation current due to the creation of functional groups (-COOH, -OH *etc.*). Peak-to-peak separation voltage decreases to 0.32 V for fZnOnF/ITO electrode compared to ZnOnF/ITO at 0.45 V. Anti-ErbB2 and BSA immobilization on ZnOnF electrode via electrostatic interactions obstructs the $[Fe(CN)_6]^{3-/4-}$ diffusion from bulk solution resulting in a decreased current (283 μA). Again, it is observed that the immobilization of Anti-ErbB2 and BSA via covalent interactions followed by oxygen plasma treatment (anti-ErbB2/fZnOnF/ITO) reduces the electrochemical current compared to fZnOnF/ITO electrode (266 μA). Conjugation of these protein molecules on ZnOnF surface perhaps acts as a barrier for electron transportation from bulk solution towards electrode resulting in decreased electrochemical current. Table S1 shows the diffusion co-efficient of various fabricated electrodes. It has been observed that the higher diffusion co-efficient (8.23×10^{-8} cm^2/s) of porous morphology ZnOnF electrode may be due to the high aspect ratio of mesoporous ZnOnF that provides an electron conduction path for transportation from bulk solution resulting in the

higher diffusion of ions towards the current collector. The diffusion of electrons due to redox conversation for porous fZnOnF electrodes has been estimated as 6.28×10^{-8} cm^2/s. The functionalized ZnO nanofibers base electrode contains –COOH groups on its surface that may obstruct electron diffusion from bulk solution compared to ZnOnF without functionalization. However, antibody functionalization on ZnOnF decreases the diffusion of electrons (3.64×10^{-8} cm^2/s) due to attachment of insulating antibody molecules on its surface. The antibody functionalized electrode using fZnOnF again shows decreased diffusion of electrons (3.13×10^{-8} cm^2/s), this may be due to covalent interaction indicating that the higher amount of antibody molecules can be attached with fZnOnF. In scan rate studies, we have measured the CV response of both fabricated bioelectrodes (anti-ErbB2/fZnOnF and anti-ErbB2/ZnOnF) as a function of scan rate [20−120 mV/s] (Figure S2, Supplementary Information). The peak-to-peak separation voltage of both bioelectrodes increases and shifts toward higher potential side with increasing scan rates. The anodic and cathodic peaks current of both bioelectrodes are found to be proportional and inversely proportional with square root of scan rate. Thus, the results these studies indicate that both biolectrodes show surface controlled process.[34] The variation of peak (anodic and cathodic) current for both bioelectrodes as a function of square root of scan rate follows Equations (1-4).

$$I_{pa}\ (\text{anti-ErbB2/ZnOnF}) = 55\mu\ [A^2\,mV^{-1}\,s]^{1/2} \times \text{Scan rate}\ [mV/s]^{1/2} + 91\ \mu A \quad (1)$$

$$I_{pc}\ (\text{anti-ErbB2/ZnOnF}) = -39\mu\ [A^2\,mV^{-1}\,s]^{1/2} \times \text{Scan rate}\ [mV/s]^{1/2} - 151\ \mu A \quad (2)$$

$$I_{pa}\ (\text{anti-ErbB2/fZnOnF}) = 43\mu\ [A^2\,mV^{-1}\,s]^{1/2} \times \text{Scan rate}\ [mV/s]^{1/2} + 83\ \mu A \quad (3)$$

$$I_{pc}\ (\text{anti-ErbB2/fZnOnF}) = -27\mu\ [A^2\,mV^{-1}\,s]^{1/2} \times \text{Scan rate}\ [mV/s]^{1/2} - 158\ \mu A \quad (4)$$

To investigate the interfacial property of electrode/electrolyte, we have carried out electrochemical impedance spectroscopy (EIS) measurements as a function of frequency

(0.01−10^5 Hz). The EIS spectra obtained for the fabricated electrodes are shown in Figure 4ii. The charge transfer resistance (R_{ct}) and constant phase element (CPE) of various electrodes has been obtained from Nyquist plots (equivalent circuit diagram shown in Figure 4iii) using EIS measurements [Table S1]. The presence of functional groups on fZnOnF surface increases the R_{ct} value; however, the CPE value is decreased compared to fZnOnF electrode. This may be due to the enhanced hydrophilic nature of ZnOnF after surface oxygen plasma treatment. Proteins (antibody and BSA) conjugation on ZnOnF surface further enhances the R_{ct} value. In addition, oxygen plasma treatment of ZnOnF electrode improves the loading of protein molecules, which hinders the diffusionof electron produced in oxidation/reduction of $[Fe(CN)_6]^{3-/4-}$ ions resulting in higher R_{ct} [451 Ω] compared to the physical absorption of protein molecules on ZnOnF electrode surface [R_{ct} : 412 Ω]. The reduction of constant phase element after protein immobilization indicates attachment of biomolecules on ZnOnF surface resulting in increased electric double layer formed between theconductive ITO electrode and an adjacent electrolyte. Interestingly, the capacitive behavior of ZnOnF electrode is changed by the incorporation of functional groups on its surface for protein conjugations. The low value of CPE for anti-ErbB2/ZnOnF immunoelectrode [2.31×10^{-5} F] indicates the higher double layer distance compared to anti-ErbB2/fZnOnF immunoelectrode [2.72×10^{-5} F].

The heterogeneous electron transfer rate constant (k_0) in presence of $[Fe\ (CN)_6]^{3-/4-}$ mediator has been determined for various fabricated electrodes as shown in Table S1. The value of k_0 can be estimated using the relation as $k_0=RT/n^2F^2AR_{ct}C$, where n is the electron transferring constant of the redox couple, F is Faraday constant, A is the area of the electrode, R is the gas constant, T is the temperature, R_{ct} is the charge transfer resistance and C is the concentration of the redox mediator. It is observed from Table S1that the highest electron

transfer rate [11.1× 10^{-7} cm/s] occurs for the pristine zinc oxide electrode, but declines for the oxy-plasma treated and antibody functionalized electrodes with or without the plasma treatment. Surface treatment of the ZnOnF electrode at the electrode/electrolyte interface could be responsible for the observed dependence of the electron-transfer kinetics of the $[Fe(CN)_6]^{3-/4-}$ mediator. Higher impedance or slower charge transfer rate of anti-ErbB2/fZnOnF immunoelectrode [47.3× 10^{-7} cm/s] results in the higher capacitance creation at the electrode surface. The surface coverage (θ) can be calculated using the relation; θ= 1-R_{ct} (electrode)/R_{ct} (bioelectrode), where θ is the fraction of occupied binding sites. The Rct (electrode) and Rct (bioelectrode) are the surface specific charge transfer resistances of the ZnOnF electrode and the antiErbB2/ZnOnF bioelectrode, respectively. We have estimated the surface concentration of physisorption and covalent attachment of the antibody on ZnOnF electrode surface as 53.6 % and 54.1% respectively. Thus, 0.5 % enhancement of surface coverage of covalently immobilized antibodies occurs on the electrode surface via plasma treatment. The surface coverage of electrode can enhance the electrochemical sensitivity and LOD of biosensor device.

Electrochemical Detection of the Cancer Biomarker. The electrochemical impedance spectroscopy (EIS) technique has been utilized for the label-free detection of human epidermal growth factor receptor 2 (ErbB2). Anti-ErbB2 was functionalized on ZnOnF electrode surface with and without the oxygen plasma treatment for detection of various concentration of ErbB2 (1.0 fM-0.5 μM). Figure 5i and ii show the EIS spectra of anti-ErbB2/ZnOnF and anti-ErbB2/fZnOnF electrodes as a function of ErbB-2 concentration. These biosensors can be regenerated by introducing glycine solution (0.2 M) of pH 2.4 for two minutes which re-generated 96.5% of the initial signal. It has been observed that the charge transfer resistance in these EIS spectra increases with increasing the concentration of ErbB-2. Figure 5iii and iv shows

the plots of charge transfer resistances (R_{ct}) and logarithmic value of ErbB-2 concentrations for anti-ErbB2/ZnOnF and anti-ErbB2/fZnOnF immunoelectrodes. Interaction of specific binding sites of antigen and antibody on transducer surface form immunocomplex layer obstructs the electron transfer from bulk solution resulting in higher R_{ct}. It has been found that the R_{ct} value for anti-ErbB2/fZnOnF electrode is higher compared to anti-ErbB2/ZnOnF [Figure 5iii], which may be due to the available functional groups created after the oxygen plasma treatment on ZnOnF surface. These fabricated immunoelectrodes can detect 1.0fM concentration of ErbB2 within a range of concentration [1.0 fM-0.5 μM or (4.34×10^{-5} - 2.17×10^{4} ng/mL)]. A comparable sensitivity for both anti-ErbB2/fZnOnF (7.76 kΩ/M/cm^2) and anti-ErbB2/ZnOnF (7.6 kΩ/M/cm^2) electrodes has been obtained. The limit of detection (LOD) for anti-ErbB2/fZnOnF is low (1.3 M) compared to the anti-ErbB2/ZnOnF (1.6) immunoelectrode. The three dimensional structure of mesoporous ZnOnF improves the loading of protein molecules such as anti-ErbB2 and BSA resulting in higher sensitivity in both cases and improved stability of the immunosensor. Myung *et al.* have developed a 3D structure of graphene based biosensor which significantly increases the surface-to-volume ratio, thereby improving the detection limits to 1.0pM for HER2 and 100 pM for EGFR breast cancer biomarkers.[30] Tehrani *et al.* have fabricated micro-channels of chemically modified multi-layer epitaxial graphene based biosensor for detection of cancer biomarker (8-hydroxydeoxyguanosine) that is sensitive to 0.35 nM concentration.[35] However, the prepared biosensors can detect lower concentration of ErbB2 compared to those of the reported biosensors (Table 1),[29, 30, 36, 37]this may perhaps be because of the high surface area of mesoporous ZnOnF for antibody conjugation. Table 1 shows the breast cancer sensing characteristics for the fabricated immunoelectrodes with the reported literature. The control experiments for ZnOnF and fZnOnF electrodes have been carried out with and

without enzyme immobilization (Figure S3, Supplementary Information). The R_{ct} values for electrodes are slightly changed in the presence of ErbB2 concentration and values are not systematic. This may be due to non-specific binding with proteins molecules in the presence of antigen solution. The detection time has been found as 128 s for oxy-plasma treat immunoelectrode (fZnOnF) compared to untreated ZnOnF immunoelectrode (141 s) as shown in Figure S4 (Supplementary Information). Compared to the other reported biosensors for the breast cancer detection, the biosensor fabricated here can detect a much lower concentration (1.0 fM) of the biomarker (Table 1). The association constant (K_a) for both fZnOnF and ZnOnF based immunoelectrodes is higher (404.8 $kM^{-1}s^{-1}$ and 165.6 $kM^{-1}s^{-1}$, respectively) compared to other immunosensors reported.[38, 39] Thus, the higher K_a of fZnOnF electrode, indicating high affinity towards ErbB2 antigen. This may perhaps be assigned to the covalent immobilization of antibody compared to ZnOnF immunoelectrode.

The reproducibility was investigated by detecting 100 nM of ErbB2 with five different immunoelectrodes with similar conditions. The relative standard deviations (RSD) for the anti-ErbB2/ZnOnF and anti-ErbB2/fZnOnF immunoelectrodes were found to be as 5.9% and 2.3%, respectively, which suggest the good precision and reproducibility of the immunosensors. The stability of the anti-ErbB2/ZnOnF and anti-ErbB2/fZnOnF was investigated for 50 days. The anti-ErbB2/fZnOnF immunosensor retained 95.5% signal from its initial value, while 88 % signal retention was observed after 50 days in the case of the anti-ErbB2/ZnOnF immunoelectrode (Figure S5, Supplementary Information). To investigate the interference of the immunosensors, the responses towards human IgG, cholesterol, PSA, glucose and also with the BSA have been determined considering its significance in serum. The immunosensors were used to test in the presence of 100 nM of ErbB2 with normal concentrations of interferents (Figure S6,

Supplementary Information). The variation of charge transfer resistance (R_{ct}) due to the interfering substances was found to be less than 5% for both immunoelectrodes, indicating good selectivity.

Conclusions

We have demonstrated the fabrication of an efficient, rapiddetection and highly sensitive label-free immunosensor using antibody anchoring electrospun mesoporous zinc oxide nanofibers. The electrospun fibrous electrode was treated with theoxygen plasma for enhancing the loading capacity of protein (antibody) molecules via EDC/NHS covalent surface chemistry. Electrochemical detection of protein functionalized fibrous immunoelectrode by impedance spectroscopic method has been carried out with and without oxy-plasma treatment on ZnOnF surface for concentration of breast cancer biomarker. In these prepared immunosensors, the free-standing mats of partially aligned ZnOnF (diameters less than 100 nm) were controlled during the synthesis of nanofibers, however, after electrophoretic deposition of these ZnOnF onto indium tin oxide surface has changed their morphological order due to high deposition potential. The electrochemical property of ZnOnF based electrode has been changed with proteins molecules. The heterogeneous electron transfer constant and diffusion coefficient of antibody conjugated ZnOnF electrode has been found to decrease that influences the impedance signal during ErbB2 detection. Thus, both fabricated immunoelectrodes (oxy-plasma treated and untreated) show a comparable analytical performance for the detection breast cancer biomarker results in insignificant change in sensitivity and significant change in heterogeneous electron

transfer rate constant, detection time and association constant. These immunosensors provide fast response as 128 s and 141 s for fZnOnF and ZnOnF bioelectrodes, respectively and are capable of detecting femto-molar concentration of ErbB2 in a wide range of 1fM-0.5 μM without using any labeling agent with good sensitivity, stability, reproducibility and selectivity. Mesoporous ZnOnF based label-free immunosensor thus provides a suitable platform for an early detection of breast cancer diagnosticsand may also find applications in an efficient detection of a host of other biomarkers.

Materials and methods

Materials.N, N dimethyl-formamide (DMF) solvent was purchased from Fischer Scientific, India. Zinc acetate (Zn $(CH_3COO)_2$, $2H_2O$, 99%), polyacrylonitrile [PAN(Mw =1,50,000)], naphthalene and anthracene were procured from Sigma–Aldrich, USA. Bovine serum albumin (BSA), N-hydroxysuccinimide (NHS), N-ethyl-N0-(3-dimethylaminopropyl carbodiimide) (EDC), were purchased from Sigma–Aldrich (USA). For stock solution of epidermal growth factor receptor, 2ErbB-2 (human recombinant), we have used 0.1M acetate buffer of pH-4 (0.5mg/ml). To dilute the stock solution of ErbB2, we have used acetate buffer (0.1M). The polyclonal antibody of ErbB2 solubility in phosphate buffered saline (PBS) containing 30% glycerol, 1% BSA and 0.02% thimerosal were found from BioVision, USA. Deionized distilled water was from Millipore water purification system. BSA (2 mg/mL) solution was prepared in 50 mM PBS (pH 7.4) containing 150 mMNaCl.

Instrumentation. The synthesized ZnOnF has been confirmed by Fourier-transform infra-red spectroscopy (FT-IR; Perkin-Elmer, Model 2000) before and after oxygen plasma treatment. The morphology shape and size of the ZnOnF at different conditions were observed by Field

emission scanning electron microscopy (FE-SEM; supra 400VP, Zeiss, Germany). The energy-dispersive X-ray spectroscopy (EDX; Oxford Instruments) analysis for elemental composition of the ZnOnF has been carried out. The X-ray diffraction (XRD; X'Pert Pro, PAN Analytical, Netherlands, X-ray system with Cu Kα radiation and λ = 1.54 Å) pattern was confirmed the crystalline structure of synthesized ZnOnF. UV−visible (Varian Cary 50Bio, UV−vis spectrophotometer) was conducted to investigate the structural properties of ZnOnF. The Brunauer Emmett Teller (BET; Quantachrome Instruments, U.S.A.) was carried out to evaluate the pore size distribution and total surface area of ZnOnF. The cyclic voltammetry, electrochemical impedance spectroscopy were performed using an Autolab Potentiostat/Galvanostat (Electrochemical analyzer; AUT-84275) in PBS at pH 7.4 containing 5 mM of $[Fe(CN)_6]^{3-/4-}$ as a mediator. Platinum (Pt) and Ag/AgCl electrodes were used for counter and reference electrodes, respectively.

Synthesis of Mesoporous ZnOnF. Synthesis of mesoporous ZnO nanofibers has been demonstrated in the previous reported paper.[33] A pictorial representation is shown in Schematic 1 and the synthesis protocol of zinc oxide nanofibers. In brief, a 7.5 wt. % PAN solution was prepared in DMF solvent and magnetically stirred for 1 h at 60 ˚C. Then, 0.25 gm of zinc acetate (ZnA) was mixed in the prepared PAN solution, and stirred for 6 h at 50 ˚C to obtain a homogenous mixture of PAN-ZnA solution. This PAN-ZnA solution was transferred to a plastic hypodermic syringe (Dispovan, Hindustan Syringes Medical Devices Ltd, India), and fed through a syringe pump (Harvard Apparatus, Holliston, MA) at 75 µL/min flow rate. An electric field (3.5 kV cm^{-1}) has been applied by a DC power source (Gamma High Voltage, Inc., High Bridge, NJ) in between the needle tip and the rotating collector. The collector was electrically

grounded and rotating at 3000 rpm. This rotating collection module consists of the rotating drum unit with a translational linear motion emitter.

The non-woven fibers were collected for ~5 h to make a thick mat (0.1 mm) on a rotating drum electrode which was covered with an aluminium foil. This free-standing mat like structure of nanofibers was then heated in air at 165 ^{o}C for 3 h for stabilization which remove the solvent and moisture present in the collected as-spun fibers. The above method was repeated by varying the parameters like concentration of PAN solution and the solution flow rate at a constant electric field. All the experiments were carried out in a controlled atmosphere at the room temperature of 25 ^{o}C, 32% humidity and at a pH value of 7). The nanofibers mat thus formed were calcined at 500 ^{o}C temperature, (ramp rate = 5 ^{o}C/min) for 2 h.

Electrode Fabrication. In order to fabricate the electrode, 3.5 mg of electrospun, partially aligned ZnOnF free-standing mat was added into 5 ml of acetonitrile and sonicated (40 W, 0.25 A) for 5 h. During electrophoretic deposition, 1 mL of ZnOnF suspended solution was added into 10 mL of acetonitrile solution and sonicated. A platinum foil (1cm×2cm) and a pre-cleaned ITO-coated glass substrate (size; 0.5 cm^2, sheet resistance; 30 Ω cm^{-1}) acted as the cathode and anode electrode, respectively. These two electrodes were positioned parallel to each other and separated by 1 cm and dipped in the ZnOnF colloidal suspension. A DC voltage of 60 V was applied between two electrodes for 3 min in presence of ZnOnF colloidal suspension. The suspended ZnOnF were deposited uniformly on ITO electrode surface due to opposite charged polarity of applied potential and ZnOnF. Then, the deposited films were removed from the ZnOnF suspension and washed several times with de-ionised water followed by drying at 100 ^{o}C. Again, the ZnOnF electrode was treated with oxygen plasma for covalent functionalization (fZnOnF) with antibody.

Device Fabrication for Breast Cancer Diagnostics. For antibody-ErbB2 functionalization, we explored both physical and covalent immobilizations. The anti-ErbB2/ZnOnF (without plasma treatment) and anti-ErbB2/fZnOnF (with plasma treatment) immunoelectrodes were used for label-free detection of epidermal growth factor receptor 2 (ErbB2; breast cancer biomarker) via antigen-antibody interactions. In physical immobilization, the antibody-ErbB2 solution (0.02 mg/mL) was directly spread over the ZnOnF surface. The physical absorption of anti-ErbB2 has been carried out without oxygen plasma treatment on ZnOnF surface.

Prior to covalent functionalization, the ZnOnF based electrodes were treated oxygen plasma at vacuum pressure was set to 0.005 mbar. The ZnOnF/ITO electrode with and without surface treatment were utilized for conjugation of the protein cancer biomarkers (anti-ErbB2) via physical absorption as well as covalent attachment. During the plasma treatment, oxidation was performed in low intensity mode for 15 min, oxidation voltage was kept at 450 V and pure oxygen was supplied. In this process, various residual organic impurities and weakly bound organic contamination could be removed from the ZnOnF/ITO surface. Thus, the plasma treatment was introduced various functional groups, such as −COOH, −OH, *etc.* on ZnOnF/ITO and confirmed using FTIR studies. The prepared electrodes were treated with EDC-NHS for 4 h to activate functional groups (-COOH) on ZnOnF electrode surface. In EDC-NHS coupling chemistry, the EDC (0.2M) works as a coupling agent while NHS (0.05M) works as an activator. This chemical treatment allowed for the binding of ZnOnF and antibody (anti-ErbB2) via covalent amide bond on fZnOnF (plasma treated) surface. Anti-ErbB2 solution (0.02 mg/mL) was spread on fZnOnF surface and kept it for overnight under humid condition (4 °C) followed by washing with phosphate buffer containing 0.05% in order to remove any unbound anti-ErbB2. The amide (C-N) bond formation between –COOH groups of fZnOnF/ITO and -NH_2 groups of

anti-ErbB2 resulting in better immobilization compared to electrostatic interaction on ZnOnF surface. BSA (2 mg/dL) was used for blocking the non-specific adsorption of anti-ErbB2. The specific binding (paratope) of anti-ErbB2 on transducer surface allows its interaction with antigen ErbB2 (epitope) resulting in a change of electrochemical signal. For the electrochemical impedance studies, the fabricated electrodes were immersed in a phosphate buffer saline (PBS) solution containing ferro/ferri cyanide mediator. Schematic 2 shows the fabrication of immunosensor and conjugation of breast cancer biomarker with surface functionalization.

ACKNOWLEDGEMENTS

We are thankful to the Department of Science and Technology (DST), New Delhi, India for their support to the Unit on Soft Nanofabrication at Indian Institute of Technology Kanpur. Authors thank Dr. Ved V. Agrawal for interesting discussion.

REFERENCES

1. A. Mishra and M. Verma, *Cancers*, 2010, 2, 190-208.
2. G. Orphanos and P. Kountourakis, *Hematol. Oncol. Stem Cell Ther.*, 2012, 5, 127-137.
3. D. Hanahan and R. A. Weinberg, *Cell*, 2011, 144, 646-674.
4. H. Zhang, A. Berezov, Q. Wang, G. Zhang, J. Drebin, R. Murali and M. I. Greene, *J. Clin. Invest.*, 2007, 117, 2051-2058.
5. A. Vasudev, A. Kaushik and S. Bhansali, *Biosensors and Bioelectronics*, 2013, 39, 300-305.
6. Breast cancer chemosensitivity, Springer, New York, USA, 2007.
7. B. V. Chikkaveeraiah, A. A. Bhirde, N. Y. Morgan, H. S. Eden and X. Chen, *ACS Nano*, 2012, 6, 6546-6561.
8. T. Y. Rakovich, O. K. Mahfoud, B. M. Mohamed, A. Prina-Mello, K. Crosbie-Staunton, T. V. D. Broeck, L. D. Kimpe, A. Sukhanova, D. Baty, A. Rakovich, S. A. Maier, F. Alves, F. Nauwelaers, I. Nabiev, P. Chames and Y. Volkov, *ACS Nano*, 2014, 8, 5682-5695.
9. R. Akter, M. A. Rahman and C. K. Rhee, *Anal. Chem.*, 2012, 84, 6407−6415.

10. K.-T. Yong, H. Ding, I. Roy, W.-C. Law, E. J. Bergey, A. Maitra and P. N. Prasad, *ACS Nano*, 2009, 3, 502–510.
11. J. Yao, M. Yang and Y. Duan, *Chem. Rev.*, 2014, 114, 6130−6178.
12. K. Mondal, M. A. Ali, V. V. Agrawal, B. D. Malhotra and A. Sharma, *ACS Appl. Mater. Interfaces*, 2014, 6, 2516−2527.
13. M. Ahmad, C. Pan, Z. Luo and J. Zhu, *J. Phys. Chem. C*, 2010, 114, 9308–9313.
14. Y. Fang, Q. Pang, X. Wen, J. Wang and S. Yang, *Small*, 2006, 2, 612–615.
15. H. Hong, J. Shi, Y. Yang, Y. Zhang, J. W. Engle, R. J. Nickles, X. Wang and W. Cai, *Nano Lett.*, 2011, 11, 3744–3750.
16. P. K. Vabbina, A. Kaushik, N. Pokhrel, S. Bhansali and N. Pala, *Biosensors and Bioelectronics*, 2015, 63, 124-130.
17. S. S. Mali, H. Kim, W. Y. Jang, H. S. Park and P. S. Patil, *ACS Sustainable Chem. Eng.*, 2013, 1, 1207-1213.
18. J. Liu, P. Pham, V. Haguet, F. Sauter-Starace, L. Leroy, A. Roget, E. Descamps, A. Bouchet, A. Buhot, P. Mailley and T. Livache, *Anal. Chem.*, 2012, 84, 3254−3261.
19. M. D. Scanlon, U. Salaj-Kosla, S. Belochapkine, D. MacAodha, D. Leech, Y. Ding and E. Magner, *Langmuir*, 2012, 28, 2251–2261.
20. P. R. Solanki, A. Kaushik, V. V. Agrawal and B. D. Malhotra, *NPG Asia Mater.*, 2011, 3, 17-24.
21. P. Si, S. Ding, J. Yuan, X. W. D. Lou and D.-H. Kim, *ACS Nano*, 2011, 5, 7617-7626.
22. C. E. Bunker, K. C. Novak, E. A. Guliants, B. A. Harruff, M. J. Meziani, Y. Lin and Y.-P. Sun, *Langmuir*, 2007, 23, 10342-10347.
23. H. S. Yoo, T. G. Kim and T. G. Park, *Adv. Drug Delivery Rev.*, 2009, 61, 1033-1042.
24. X. Ren, D. Chen, X. Meng, F. Tang, X. Hou, D. Han and L. Zhang, *J. Colloid Interface Sci.*, 2009, 334, 183-187.
25. R. S. Kane and A. D. Stroock, *Biotechnol. Prog.*, 2007, 23, 316-319.
26. K. Mondal, S. Bhattacharyya and A. Sharma, *Ind.Eng.Chem. Res.*, 2014, 53, 18900–18909.
27. X. Xu, B. Z. Tian, J. L. Kong, S. Zhang, B. H. Liu and D. Y. Zhao, *Adv. Mater.*, 2003, 15, 1932-1936.
28. H. Hong, J. Shi, Y. Yang, Y. Zhang, J. W. Engle, R. J. Nickles, X. Wang and W. Cai, *Nano Lett.*, 2011, 11, 3744–3750.
29. C. Baj-Rossi, G. D. Micheli and S. Carrara, *Sensor*, 2012, 12, 6520-6537
30. S. Myung, A. Solanki, C. Kim, J. Park, K. S. Kim and K.-B. Lee, *Adv. Mater.*, 2011, 23, 2221–2225.
31. G. Rodríguez-Gattorno, P. Santiago-Jacinto, L. Rendon-Vázquez, J. Németh, I. Dekany and D. Diaz, *J. Phys. Chem. B*, 2003, 107, 12597–12604.
32. M. E. Aguirre, H. B. Rodríguez, E. S. Roman, A. Feldhoff and M. A. Grela, *J. Phys. Chem. C*, 2011, 115, 24967-24974.
33. P. Singh, K. Mondal and A. Sharma, *J. Colloid Interface Sci.*, 2013, 394, 208-215.

34. S. Srivastava, M. A. Ali, P. R. Solanki, P. M. Chavhan, M. K. Pandey, A. Mulchandani, A. Srivastava and B. D. Malhotra, *RSC Advances*, 2013, 3, 228-235.
35. Z. Tehrani, G. Burwell, M. A. M. Azmi, A. Castaing, R. Rickman, J. Almarashi, P. Dunstan, A. M. Beigi, S. H. Doak and O. J. Guy, *2D Mater.*, 2014, 1, 025004.
36. J. T. Gohring, P. S. Dale and X. Fan, *Sensor Actuat.*, 2010, 146, 226-230.
37. N. A. Mansor, Z. M. Zain, H. H. Hamzah, M. S. A. Noorden, S. S. Jaapar, V. Beni and Z. H. Ibupoto, *Open J. Appl. Biosen.*, 2014, 3, 9-17.

Transducers	Biomarkers	Techniques	Sensitivity	Detection Limit	Test range	Association constant (K_a)	Reference

38. M. A. Ali, S. Srivastava, M. K. Pandey, V. V. Agrawal, R. John and B. D. Malhotra, *Anal. Chem.*, 2014, 86, 1710-1718.
39. Z. Matharu, A. J. Bandodkar, G. Sumana, P. R. Solanki, E. M. I. M. Ekanayake, K. Kaneto, V. Gupta and B. D. Malhotra, *J. Phys. Chem. B*, 2009, 113, 14405-14412.
40. Y. Zhu, P. Chandra and Y.-B. Shim, *Anal. Chem.*, 2013, 85, 1058−1064.

Table 1: Sensing performances of fabricated electrodes with reported literature for breast cancer biomarker detection.

Reduced graphene oxide-coated SiO_2 NPs	HER2	FET-type	…….	1 pM	1 $pM^{-1}\mu M$	……..	Myung *et al*[30].
Opto-fluidic ring resonator	HER2	Optical	30 nm/RIU	sub-ng/mL	13 - 100 ng/mL	……	Gohring *et al*[36].
ZnO nanowires	DNA based	Electrochemical	6.36 µA/µM	3.32 µM	10.0 - 100.0 µM	…….	Mansor *et al*[37].
Hydrazine−AuNP−aptamer	HER2	Electrochemical	1.117 µAmL/ng	0.037 pg/mL	……	……..	Zhu *et al*[40].
Carbon nanotube	Anti-breast cancer agent	Electrochemical	8–925 nA/µM	13.8 µM	40-160 µM	…….	Baj-Rossi *et al*[29].
ZnOnF	ErbB2	Impedance	7.6 kΩ/ µM	1.0 fM or 4.34×10^{-5}ng/mL	1fM-0.5 µM (4.34×10^{-5} - 2.17×10^{4}ng/mL)	165.6 $kM^{-1}s^{-1}$	Present Work
fZnOnF	ErbB2	Impedance	7.76 kΩ/µM	1.0 fM	1fM-0.5 µM	404.8$kM^{-1}s^{-1}$	Present Work

Figure captions

Figure 1. FESEM micrographs for PAN/zinc acetate fibers electrospun at 75 µL/min constant flow rate with different PAN concentration, (a) beaded and non-uniform PAN/ZnA fibers observed at 3 Wt.%, (b) more uniform diameter, bead-free fibers at 7.5 wt.% and (c) higher

magnification image of 'c'. (d) Thicker fibers at 14 wt. %. Morphology of a 7.5 wt.% PAN/ZnA blend electrospun at different flow rate, (e) 15 μL/min and (f) 150 μL/min.

Figure 2.FESEM images of ZnOnF produced at calcination temperature 500 °C, (a) low magnification view of the calcined ZnO nanofibers free-standing mat, (b) higher magnification view of the ZnO mat and (c) individual high resolution image of ZnOnF. (d) FESEM for ErbB2 antibody loading on ZnOnF surface and (e) its higher magnification. TEM micrograph of ZnOnF (f), inset shows individual ZnOnF.

Figure 3.(i) X-ray diffraction of synthesized zinc oxide nanofibers calcined at 500 °C, inset shows the electron diffraction pattern of ZnOnF. (ii)FT-IR spectra of various fabricated electrodes and (iii) absorption spectra of ZnOnF; inset: Tauc plot for the band gap calculation. (iv) BET data for ZnOnF (inset: pore size distribution).

Figure 4: Cyclic voltammetric studies for various electrodes and immunoelectrodes at 20 mV/s (i), electrochemical impedance analysis for the fabricated electrodes (ii) and equivalent circuit model for a typical Nyquist plot for impedance studies.

Figure 5: Impedance spectra for anti-ErbB2/ZnOnF (i) and anti-ErbB2/fZnOnF (ii) immunoelectrodes as a function of ErbB2 concentration [1.0 fM-0.5 μM]. Sensor calibration plots for (iii) anti-ErbB2/ZnOnF and (iv) anti-ErbB2/fZnOnF immunoelectrodes using logarithmic scale.

Schematic 1. Synthesis of electrospun ZnOnF using a rotating drum collector.

Schematic 2: Immunosensors fabrication for label-free detection of breast cancer biomarker.

Figure 1

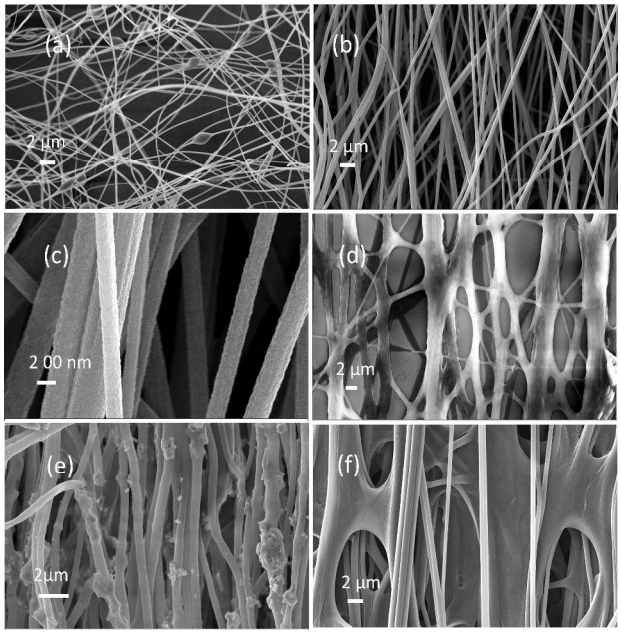

Figure 2

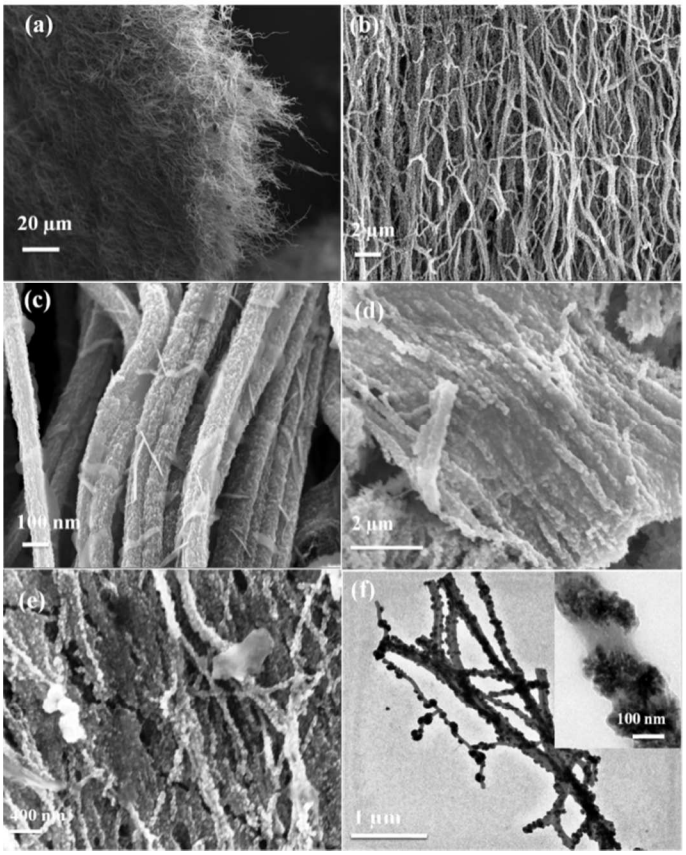

Figure 3

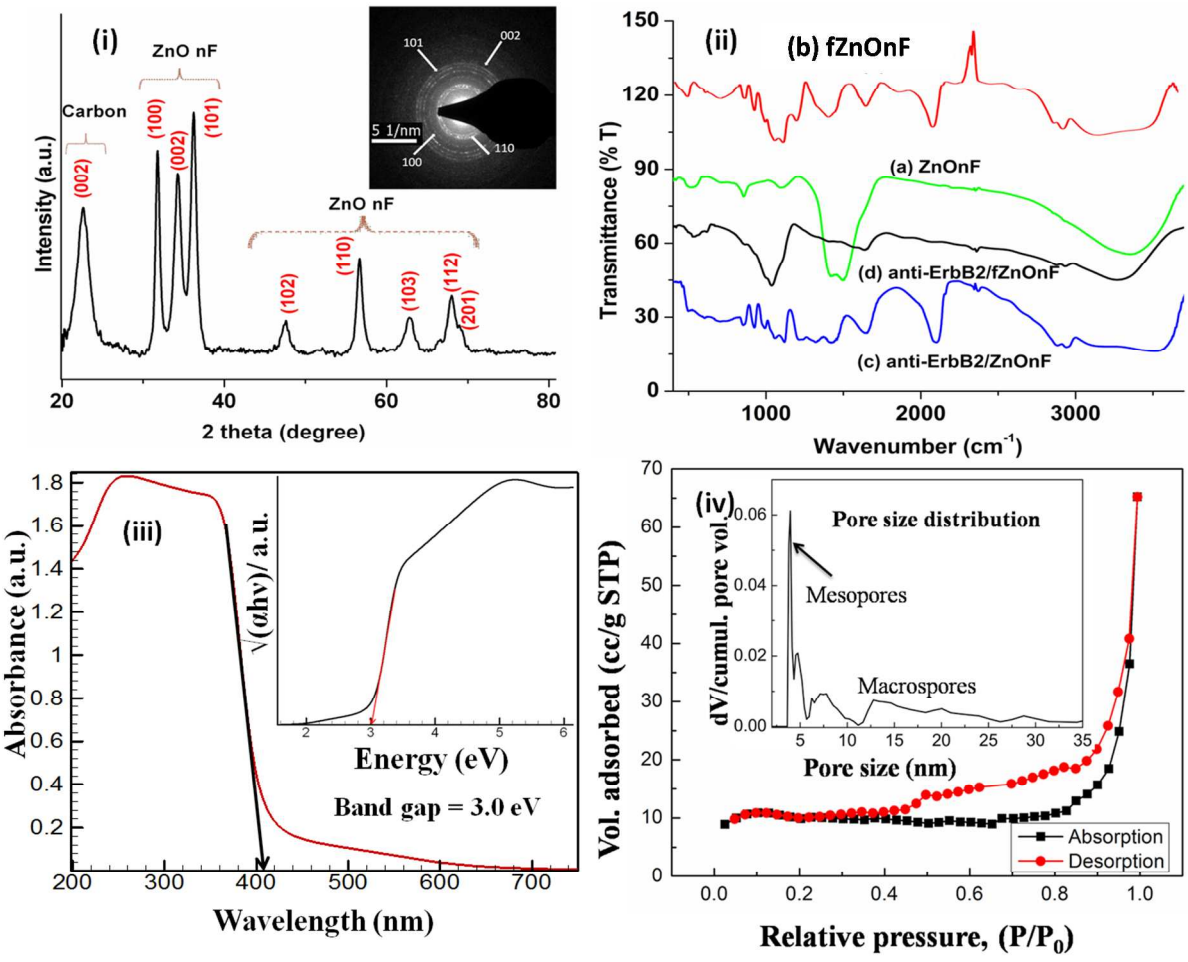

Figure 4

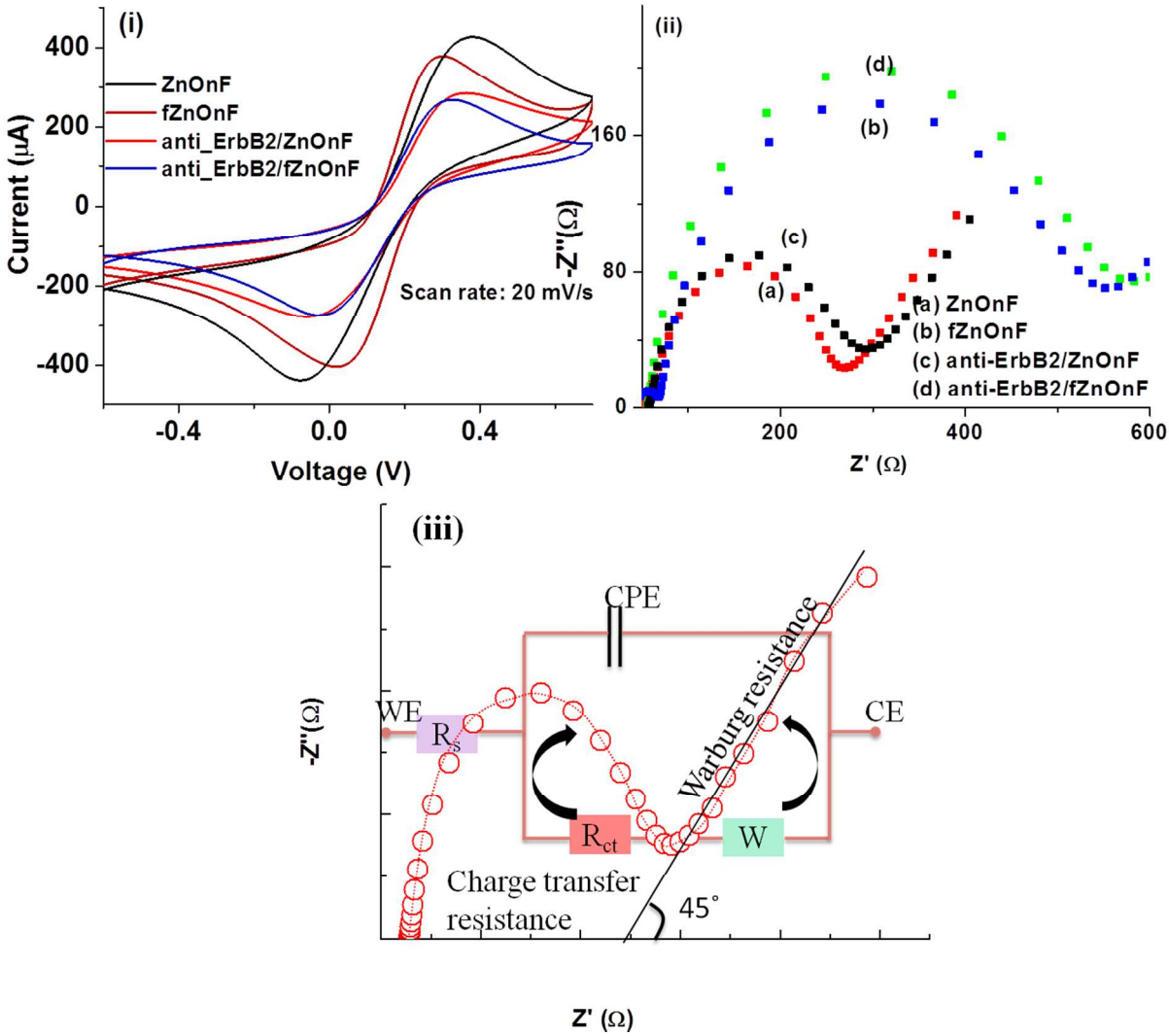

Figure 5

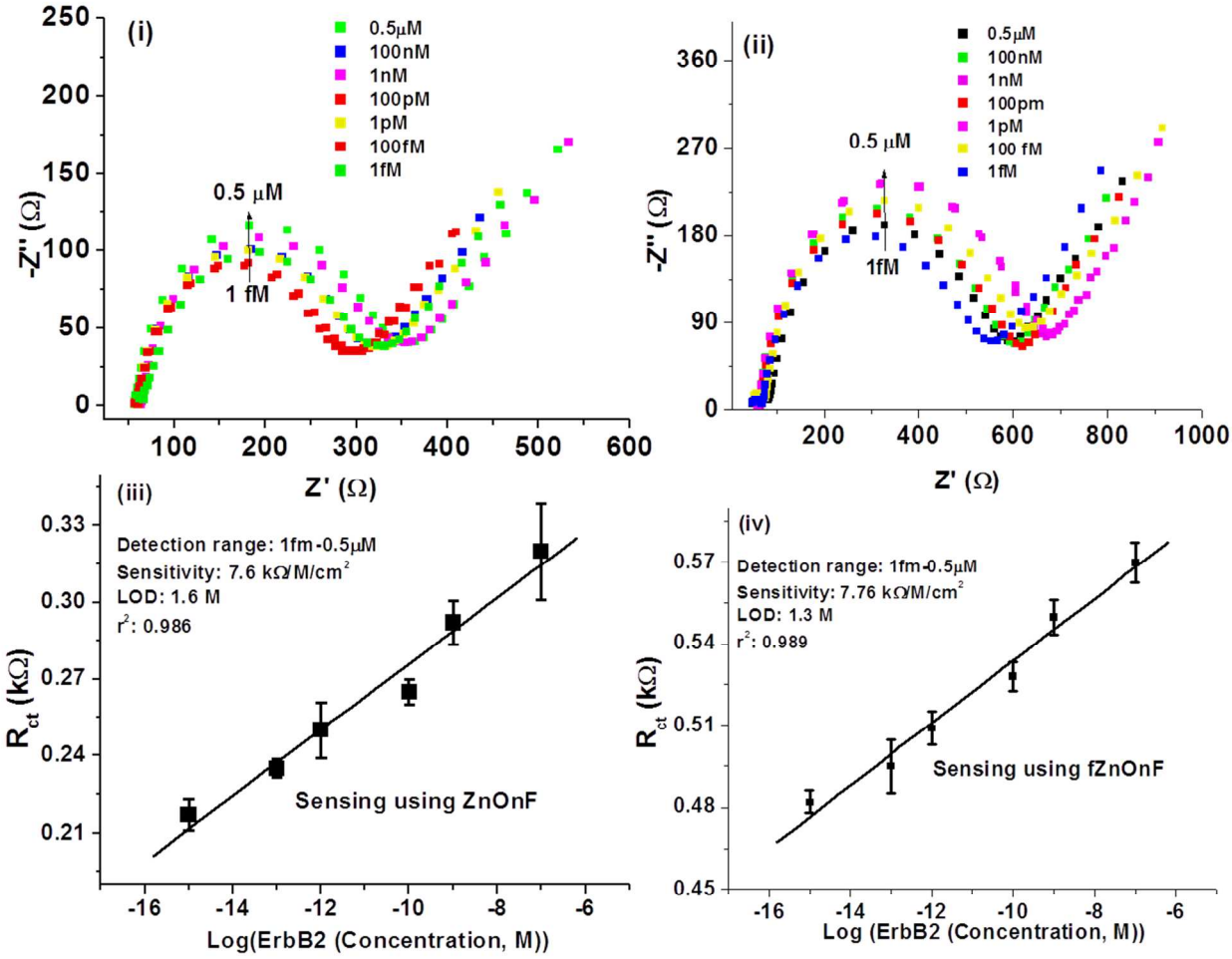

Schematic 1

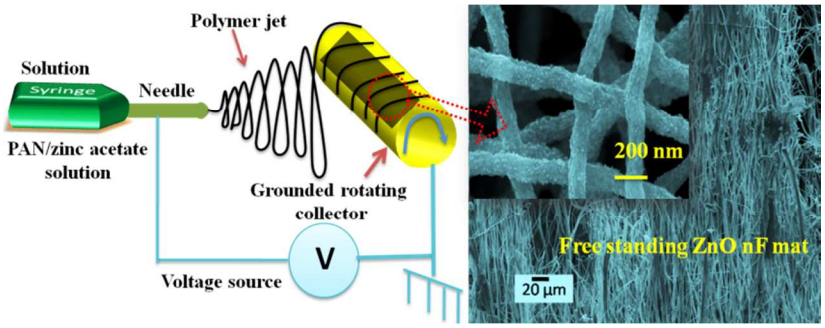

Schematic 2

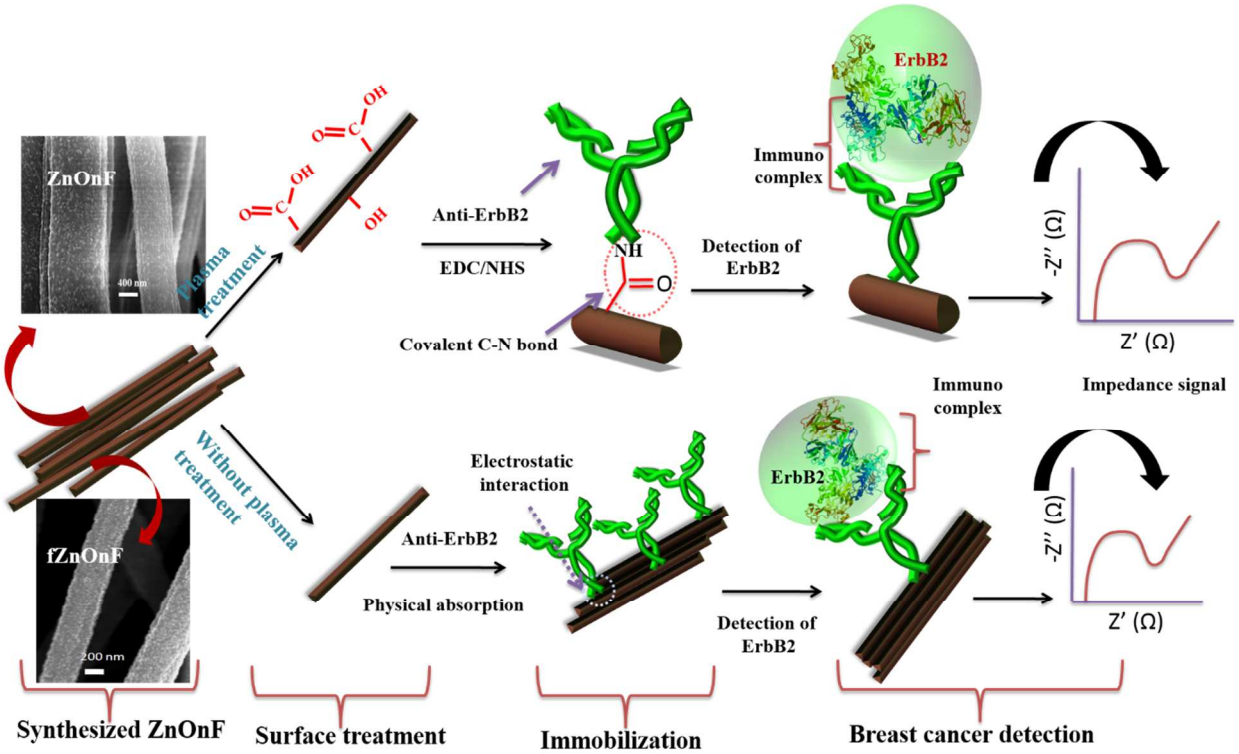

Graphical Abstract